

# Supersolidity of polariton condensates in photonic crystal waveguides

Davide Nigro,<sup>1,\*</sup> Dimitrios Trypogeorgos,<sup>2</sup> Antonio Gianfrate,<sup>2</sup>  
Daniele Sanvitto,<sup>2</sup> Iacopo Carusotto,<sup>3</sup> and Dario Gerace<sup>1</sup>

<sup>1</sup>*Dipartimento di Fisica, Università di Pavia, via Bassi 6, I-27100 Pavia, Italy*

<sup>2</sup>*CNR Nanotec, Institute of Nanotechnology, via Monteroni, 73100, Lecce, Italy*

<sup>3</sup>*INO-CNR Pitaevskii BEC Center and Dipartimento di Fisica, Università di Trento, 38123 Povo, Italy*

Condensation of exciton-polaritons has been recently observed in one-dimensional photonic crystal waveguides, exploiting the interplay of long-lived gap confined eigenmodes and negative mass polariton branches. Here we focus on the theoretical emergence of a second emission threshold, in addition to the one associated with condensation at zero-momentum, due to the nonlinear polariton scattering from the condensate into finite momentum eigenmodes. The physics of this spatially modulated condensate is related to a spontaneous breaking of both phase and translational symmetries simultaneously, bearing strong similarities with the highly sought supersolid phase in Helium and ultracold atomic gases but with a novel mechanism typical of the driven-dissipative scenario. We then propose clear-cut and unequivocal experimental signatures that would allow to identify supersolidity phenomena in polariton condensates.

**Introduction.** Exciton-polaritons are elementary excitations arising from the strong coupling between photonic and excitonic eigenmodes in low-dimensional semiconductor nanostructures [1]. Such low-dimensional polariton excitations inherit the best of two worlds: the low photon effective mass, and the strong exciton nonlinearity, making them appealing candidates for applications in nonlinear photonics [2–4], and, on a more fundamental level, for studies of quantum fluid behaviors, such as condensation and superfluidity in a novel non-equilibrium scenario that is peculiar of driven-dissipative systems [5–10]. Intense efforts have been later directed towards laterally confining microcavity polaritons, with the aim of achieving condensation and superfluidity at lower thresholds [11–15]. In this context, photonic crystal waveguides with embedded excitonic materials have been proposed as promising candidates to engineer exciton-polariton dispersion and losses [16–18]. In fact, low-threshold polariton condensation has been recently achieved in one-dimensional photonic crystal (1DPC) waveguides with embedded QWs [19], following earlier indications of condensation in gap solitons of fully etched microcavity samples with in-plane periodicity [20, 21]. It has been later shown that polariton condensation is actually achieved in gap-confined spatially quantized eigenmodes, facilitated by the creation of an effective potential well for negative mass polaritons induced by the exciting laser spot [22]. Hence, theoretical models of out-of-equilibrium condensation in a multi-band exciton-photon coupled system with symmetry-dependent losses have emphasized the crucial role played by the simultaneous presence of negative mass and energy gap in reaching the condensation threshold [23, 24].

In the present Letter we focus on power regimes above the polariton condensation threshold, exploring the interplay between condensation and further nonlinear polariton-polariton scattering processes. We theoretically anticipate the existence of a second emission thresh-

old favouring the scattering from the polariton condensate at zero momentum to equal energy side-branches at finite wave vector. Under suitable conditions, the resulting steady state configuration displays peculiar spatially modulated patterns, whose key features can be understood in terms of a spontaneous breaking of both phase and translational symmetries occurring simultaneously. In particular, such a behavior is hereby assessed as an emergent supersolid state, the latter being an elusive phase of matter that has sparked widespread interest in the last decade, especially in connection with the long-standing controversy about its observation in Helium [25] and its recent realization in ultracold atomic clouds [26–30]. Here we provide a novel playground to explore the physics of such an exotic condensed matter state in the context of driven-dissipative systems.

**Model and theory.** The scheme considered in this work is summarized in Fig. 1a, along the lines of the polariton devices analyzed in Ref. [22], and consists of a dielectric waveguide driven by a continuous wave (cw) non-resonant source impinging at normal incidence. The top surface is characterized by a periodic corrugation, e.g. along the  $x$  coordinate, and is assumed to be uniform in the transverse direction  $y$ . In this scenario, as recently shown in [22], the emission properties associated to the onset of polariton condensation can be captured by means of an effective 1D theory accounting for only the band structure along the grating direction [23]. Specifically, we assume to have a pair of photonic modes labelled as  $m = 0$  and  $m = 1$  in the following. Due to the periodic corrugation, these guided modes are folded around the horizontal wave vector origin,  $k_x = 0$  (i.e., normal incidence) within the first Brillouin zone defined by the 1DPC lattice periodicity [31], as schematically illustrated in Fig. 1b. In particular, close to  $k_x = 0$  these photonic bands display an almost linear energy-wave vector dispersion, which allows us to further classify each branch as propagating ( $l = +$ ) or counter-propagating ( $l = -$ ),

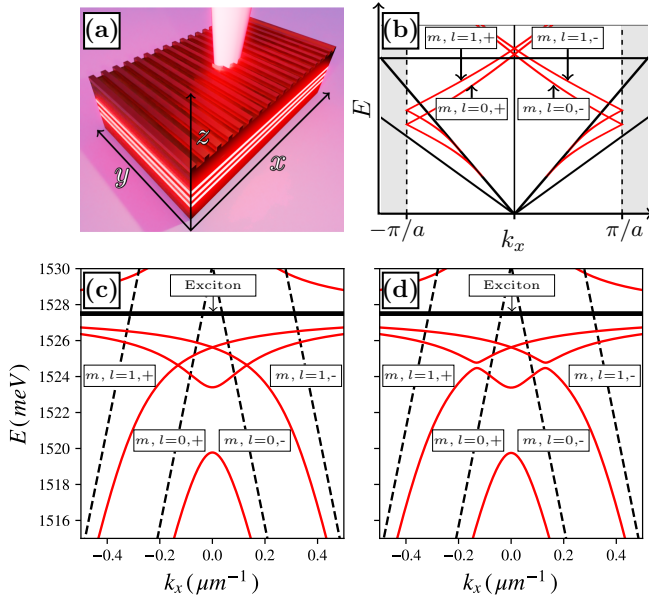


Figure 1. **(a)**: Artistic view of the proposed setup for polariton supersolidity: a dielectric waveguide with embedded excitonic material along  $z$  is periodically patterned along the  $x$ -direction (1DPC waveguide) with lattice parameter  $a$ , uniform in the  $y$ -direction, and vertically pumped by an off-resonant cw source. **(b)**: Sketch of the photonic energy-wavevector dispersion along  $x$ : a pair ( $m = 0, 1$ ) of propagating (+) and counter-propagating (-) bare photonic eigenmodes supported by the waveguide is folded within the 1DPC Brillouin zone (red lines), the total internal reflection condition lying between the core and the upper cladding (air) light lines (black oblique lines). **c – d**: Polariton dispersions (red lines) generated by the strong coupling of the bare photonic eigenmodes with QW excitons with resonance at 1527.5 meV (thick horizontal line), for (c)  $\hbar U_{0,1} = 0$  and (d)  $\hbar U_{0,1} = 1$  meV, respectively. For comparison, the dispersion of the bare photonic branches shown in panel (a) is reported with dashed lines in panels (c) and (d). Calculation parameters have been chosen according to typical values for III-V semiconductor heterostructures [22].

depending on the sign of its slope (see, e.g., Fig. 1b). In addition, the 1DPC potential may further induce a linear coupling between the  $m = 0$  and  $m = 1$  modes, e.g., when these branches have the same mirror reflection symmetry with respect to the vertical ( $x, z$ ) plane [31]. When the  $(m, l)$  modes are additionally coupled to an excitonic resonance (thick horizontal line in Figs. 1b), the dispersion is actually modified to polariton branches around  $k_x = 0$  [16, 32].

In this scenario, steady state properties of the system are determined by the long time balance between gain and losses of polariton excitations [33]. Here we consider a treatment generalizing previous works [22, 23], accounting for the presence of two photonic eigenmodes, and based on the steady state behavior of the following

set of coupled equations

$$\dot{n}_I = -\gamma_I n_I + \gamma_{A \rightarrow I} n_A + P(x), \quad (1a)$$

$$\dot{n}_A = -\gamma_A n_A + \gamma_{I \rightarrow A} n_I - g n_A \langle \vec{\psi}, G \vec{\psi} \rangle, \quad (1b)$$

$$\dot{\vec{\psi}} = -\frac{i}{\hbar} H(x) \vec{\psi} - \Gamma \vec{\psi} + \frac{g}{2} n_A G \vec{\psi} - \frac{i}{\hbar} g_{xx} \vec{W}[\vec{\psi}] + \vec{\xi} \quad (1c)$$

in which  $n_I \equiv n_I(x, t)$  is the inactive reservoir density,  $n_A \equiv n_A(x, t)$  the active one, while  $\vec{\psi} \equiv \vec{\psi}(x, t)$  is the multi-component (vector) wavefunction describing the relevant photonic and excitonic modes. In particular, here we account for 8 different components in  $\vec{\psi}$ : 4 photonic,  $A_{m,l} \equiv A_{m,l}(x, t)$ , and 4 excitonic,  $X_{m,l} \equiv X_{m,l}(x, t)$ , with  $m = 0, 1$  and  $l = \pm$  as specified in Fig. 1. The non-resonant cw source, described as  $P(x) = P_0 \exp\{-(x^2)/(2\sigma^2)\}$ , injects particles into the inactive reservoir (i.e., high-energy excitations created by the pump). The active reservoir density,  $n_A$ , accounts for excitations satisfying the proper energy-momentum conditions to be converted into polaritons. In order to allow for population exchange between the reservoirs and to account for particle losses, we included two different gain terms and two particle decay channels, respectively. In particular, the former are described by  $\gamma_{A \rightarrow I}$  and  $\gamma_{I \rightarrow A}$ , while the latter by the rates  $\gamma_I$  and  $\gamma_A$ . Particle transfer from  $n_A$  to polariton excitations is made possible by the presence of the two terms proportional to  $g$ : the one in Eq. 1b is responsible for the depletion of the reservoir whenever some particle population is stored into  $\vec{\psi}$ , with  $\langle \vec{\psi}, \vec{\psi}' \rangle = \sum_j \psi_j^* \psi'_j$  denoting the standard hermitian scalar product. Particles scattered by the active reservoir are fed into the polariton subsystem by the gain term in Eq. 1c, in which  $G$  is a  $8 \times 8$  matrix satisfying the constraints already discussed in Ref. [23]. The steady state polariton configuration is obtained by considering the time evolution of  $\vec{\psi}$  in Eq. 1c in the presence of a small amplitude random noise,  $\vec{\xi} \equiv \vec{\xi}(x, t)$ , and it is ultimately determined by the competition between the system Hamiltonian,  $H(x) = H_0(x) + V(x, t)$ , the loss matrix,  $\Gamma$ , and the nonlinear scattering term,  $g_{xx} \vec{W}[\vec{\psi}]$ . Here,  $g_{xx}$  describes the exciton-exciton resonant interaction [8], and it is assumed as an input parameter in our model. The  $H_0(x)$  term in  $H$  describes the linear polariton band structure, i.e., in the absence of nonlinear effects. In particular, as detailed in the following, a crucial role in our discussion is played by the possible presence of a linear coupling matrix element,  $U_{0,1}$ , between  $m = 0$  and  $m = 1$  branches. The corresponding Hamiltonian term reads

$$H_{0,1} = \hbar U_{0,1} (A_{0,+}^* A_{1,-} + A_{0,-}^* A_{1,+} + h.c.). \quad (2)$$

In the absence of linear coupling, the diagonalization of  $H_0$  yields the polariton branches shown in Fig. 1c, while a different band structure is obtained for  $U_{0,1} \neq 0$ , as shown in Fig. 1d, in which small energy gaps at finite

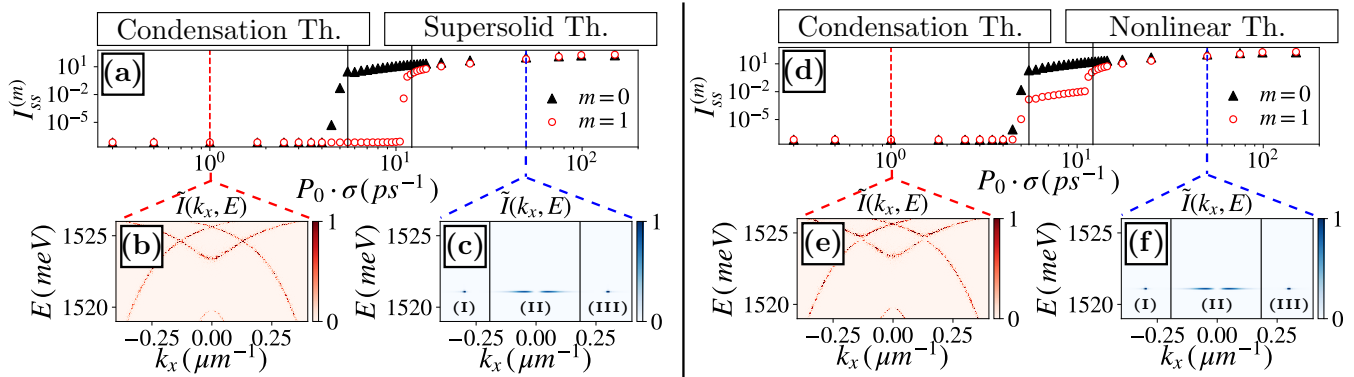


Figure 2. Numerical results obtained for  $g_{xx} \neq 0$  and  $U_{0,1} = 0$  (left panels), showing (a) the steady-state photonic emission,  $I_{ss}^{(m)}$  ( $m = 0, 1$ ), as a function of the injection rate,  $P_0 \cdot \sigma$  ( $\sigma = 10 \mu\text{m}$ ), (b) the spectrally resolved emission normalized to the peak intensity, i.e.  $\tilde{I}(k_x, E) = I(k_x, E)/\max(I(k_x, E))$ , for  $P_0 \cdot \sigma = 1 \text{ ps}^{-1}$  (i.e., below condensation threshold), and (c) for  $P_0 \cdot \sigma = 50 \text{ ps}^{-1}$  (above the supersolid transition threshold); all the other model parameters are reported in the SM file, for completeness. In panels (d),(e),(f) we report the same quantities as in (a),(b),(c), respectively, but assuming a linear coupling matrix element  $\hbar U_{0,1} = 1 \text{ meV}$ . We notice that in panels (c) and (f), the spectrally resolved emission is normalized to each peak in zones I (III) and II, respectively; The actual ratio between peak emission in region I (III) and II is about 6.

wavevector appear. Full details about the matrix representation of  $H_0$  on the  $\vec{\psi}$  basis is given in the supplemental material. The effective nonlinear coupling between  $m = 0$  and  $m = 1$  polaritons is mediated by exciton-exciton interactions (i.e., here quantified by  $g_{xx}$  in our model). Explicitly, the component  $\alpha \equiv (m, l)$  of  $\vec{W}[\vec{\psi}]$  is given by the functional derivative (we refer to the SM file for a complete account of the model details)

$$(\vec{W}[\vec{\psi}])_\alpha = \frac{\delta}{\delta \psi_\alpha^*} \int dx (X_{0,+}^* X_{0,-}^* - X_{1,+} X_{1,-} + h.c.) \quad (3)$$

**Results.** In experiments, the onset of polariton condensation is typically identified by characterizing the intensity of the radiation emitted from the sample and its emission spectrum, the latter being accessible in energy-momentum resolved measurements. In our theoretical framework, these observables correspond to the steady-state integrated emission associated to the  $m$ -th photonic component, i.e.,

$$I_{ss}^{(m)} = \lim_{t \rightarrow \infty} \int dx |A_{m,out}(x, t)|^2, \quad (4)$$

and the Fourier transform of the output field,  $A_{out}(x, t)$ , performed over a finite time window deep in the steady-state regime, i.e.,  $I(k_x, E) = |A_{out}(k_x, E)|^2$  (we refer to Ref. [23] for details). In particular, by assuming a linear coupling to the environment (as in input-output theory), we define the total output field,  $A_{out}(x, t)$ , as the spatial interference of the output fields associated to each photonic component, i.e.,

$$A_{out} = \sum_m A_{m,out}, \quad A_{m,out} \propto \sum_{l=\pm} A_{m,l}, \quad (5)$$

in which the space and time dependence are implicitly assumed.

We show in Fig. 2 numerical results for (i) the integrated emission as a function of input power, and (ii) the spectrally resolved emission at a given power, obtained either without ( $U_{0,1} = 0$ ) or with ( $U_{0,1} \neq 0$ ) linear coupling between  $m = 0$  and  $m = 1$  bare photonic eigenmodes, always assuming  $g_{xx} \neq 0$ . The two cases are directly compared by looking at Figs. 2a and 2d: in both cases, the integrated emission coming from  $m = 0$  modes displays a threshold-like behavior (black markers), i.e., a typical signature of polariton condensation, while a very different trend is observed for the integrated emission from the  $m = 1$  polariton components only (red markers). In particular, when  $U_{0,1} = 0$  the  $m = 1$  polariton mode emission shows a single nonlinear threshold as a function of input power (Fig. 2a). This threshold is related to the onset of nonlinear scattering from the condensate into  $m = 1$  modes. In contrast, as suggested by results shown in Fig. 2d, for  $U_{0,1} \neq 0$  the  $m = 1$  component emission is characterized by the presence of two thresholds: the first one coincides with the condensation threshold of  $m = 0$  polaritons into gap-confined modes, while the second threshold appearing at higher injection rates is again related to nonlinear processes involving isoenergetic scattering from  $m = 0$  to  $m = 1$  polariton states.

As a further comparison, we notice that below condensation threshold (Figs. 2b and 2e), the spectrally resolved emission clearly reproduces the polariton dispersion as reported in Figs. 1c and 1d, respectively. In particular, it is worth noting the negligible emission of the lowest polariton branch at  $k_x = 0$ , arising from the symmetry-protected bound state in the continuum nature of the

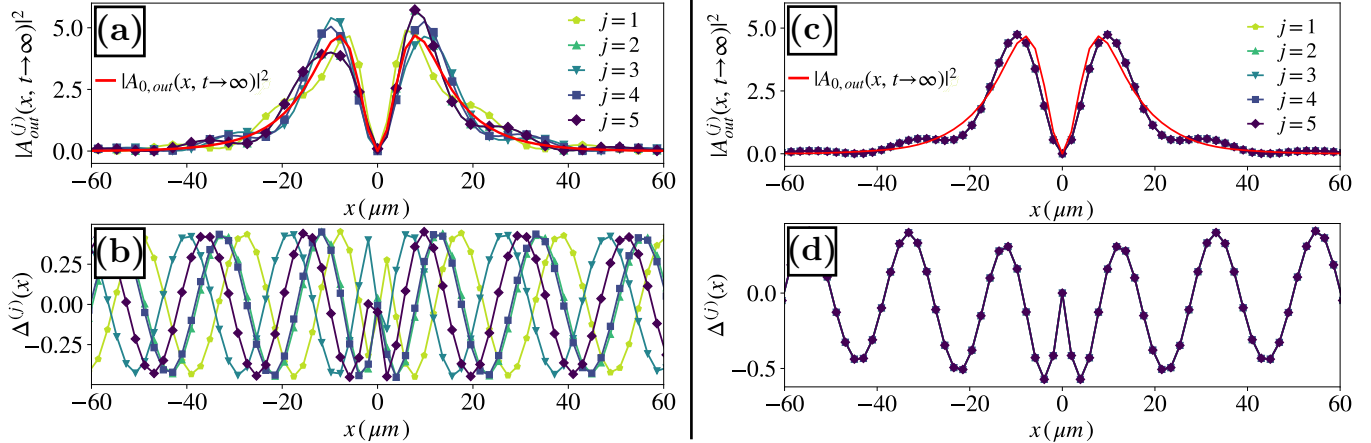


Figure 3. Numerical results obtained for  $U_{0,1} = 0$ ,  $P_0 \cdot \sigma = 50 \text{ ps}^{-1}$  (left panels), and showing (a) the total steady state emission patterns in real space,  $|A_{out}^{(j)}(x, t \rightarrow \infty)|^2$  (the solid red line only represents the steady-state emission associated to the condensate component,  $|A_{0,out}(x, t \rightarrow \infty)|^2$ ), and (b) the steady-state modulations as a function of the position,  $\Delta^{(j)}(x)$ . Data in each panel correspond to 5 different and independent stochastic time evolutions ( $j = 1, \dots, 5$ ). In panels (c),(d) we report the very same quantities as in panels (a),(b), respectively, by assuming a non-negligible linear coupling between photonic branches,  $\hbar U_{0,1} = 1 \text{ meV}$  (all the curves for different  $j$  are superimposed).

photonic mode, as already shown and thoroughly discussed [19, 22–24]. We also notice the small gaps at finite  $k_x$  in Fig. 2e (to be compared to Fig. 1d), due to  $U_{0,1} \neq 0$ . On the other hand, the emission spectrum above the second threshold reveals the presence of secondary peaks at  $\bar{k}_x \simeq 0.3 \mu\text{m}^{-1}$ , manifesting the onset of a stationary nonlinear scattering process from the  $m = 0$  condensate to the  $(1, \pm)$  propagating modes. We also notice that numerical results obtained for  $U_{0,1} = 0$  and  $g_{xx} = 0$  show no  $(1, \pm)$  emission above condensation threshold, at any injected power, as reported in Fig. S1 of the SM file, for completeness. Here, emission above the second threshold is clearly peaked in momentum space, both in Figs. 2c and f, which is intuitively associated to the presence of (almost) periodic modulations in real space. This regular pattern is accompanied by a spontaneous breaking of both phase and translational symmetries in the case  $U_{0,1} = 0$ . Indeed, this double symmetry breaking is reminiscent of the physics related to the supersolid phase transition [25, 30], here extended to an out-of-equilibrium context. However, this is a peculiar feature that cannot be directly inferred from energy-momentum resolved measurements.

To support the last interpretation, we report in Fig. 3 the outcome of 5 independent realizations ( $j = 1, \dots, 5$ ) leading to the steady-state, either for  $U_{0,1} = 0$  (left panels) or  $\hbar U_{0,1} \neq 0$  (right panels), respectively. The steady state behavior is calculated at an injection rate  $P_0 \cdot \sigma = 50 \text{ ps}^{-1}$ , i.e., corresponding to an input power above the second threshold (see Fig. 2 and SM file). We notice that we considered a cw source with  $\sigma = 5 \mu\text{m}$  for these simulations, to directly compare to spatial emission

profiles in Ref. [22]. In Figs. 3a and 3c we compare the total steady state emission profiles to  $|A_{0,out}(x, t \rightarrow \infty)|^2$  (red solid line, corresponding to the emission from the condensate only). In both situations, the total emission follows the envelope provided by the  $m = 0$  mode. However, for  $U_{0,1} = 0$  the spatial patterns evidently differ from each other for different  $j$ , due to the arbitrary phase difference between  $m = 0$  and  $m = 1$  emitted fields. This is an unequivocal signature of phase symmetry breaking. This is further evidenced by considering the long time behavior of the modulations around the  $m = 0$  emission for different configurations, quantified by the quantity

$$\Delta^{(j)}(x) = \lim_{t \rightarrow \infty} \frac{|A_{out}^{(j)}|^2 - |A_{0,out}^{(j)}|^2 - |A_{1,out}^{(j)}|^2}{|A_{0,out}^{(j)}|}. \quad (6)$$

By construction,  $\Delta^{(j)}(x)$  gives information about the interference pattern created by the superposition of  $m = 0$  and  $m = 1$  emissions, respectively. The modulation profiles associated to the 5 trajectories reported in Fig. 3a,c are then shown in Figs. 3b and 3d, respectively. In both cases, apart from the region where emission is dominated by the dark character of the condensate (i.e., around  $x = 0$ ), the spatial period of the modulations is compatible with  $2\pi/\bar{k}_x \simeq 21 \mu\text{m}$ . We also notice that this spatial periodicity is totally unrelated from the 1DPC one, which is typically  $a \sim 0.25 \mu\text{m}$  [22]. Moreover, the spatial periodicity of this polariton supersolid is determined by the energy-wavevector dispersion of the  $m = 1$  polariton branches, through the wavevector of the isoenergetic mode that is resonant with the  $m = 0$  condensate. This peculiar aspect differentiates this out-of-equilibrium

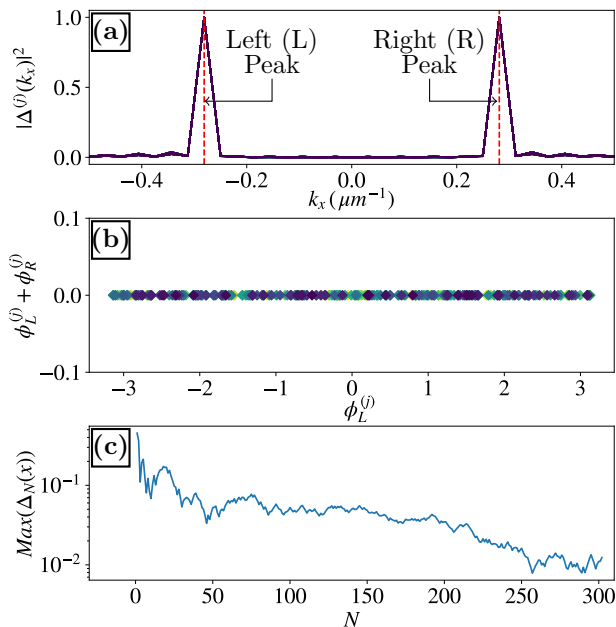


Figure 4. Here we set  $U_{0,1} = 0$  (with  $P_0 \cdot \sigma = 50 \text{ ps}^{-1}$ ), and report numerical results for **(a)** the spectral components,  $|\Delta^{(j)}(k_x)|^2$ , associated to 300 different steady-state configurations,  $\Delta^{(j)}(x)$ ; **(b)** the sum of the Left and Right peaks phases ( $\phi_L^{(j)} + \phi_R^{(j)}$ ) as function of the Left peak phase,  $\phi_L^{(j)}$  (each point corresponding to a different simulation), and **(c)** maximum of the average spatial modulation,  $\text{Max}(|\Delta_N(x)|)$  (see Eq. 8) as a function of the configuration number,  $N$ .

supersolid from realizations reported in ultracold atomic gases, in which the periodicity is solely determined by the interaction terms. In addition, here the point of the  $m = 1$  branch dispersion at which the nonlinear scattering occurs can be controlled through the input power (i.e., through the blue shift of the condensate), as we have verified numerically (not shown here, see also schematic illustration in Fig. S3 of the SM file).

For  $U_{0,1} = 0$  the modulations on top of the condensate are characterized by different phases, which is understood by taking a closer look at the Hamiltonian terms in Eqs. 2 and 3, respectively. When the  $m = 0$  and  $m = 1$  are nonlinearly connected (i.e., considering Eq. 3), the system evolution is invariant under the following phase transformation

$$Y_{1,+} \rightarrow e^{i\phi_L} Y_{1,+}, \quad Y_{1,-} \rightarrow e^{i\phi_R} Y_{1,-} \quad (Y = A, X) \quad (7)$$

for any possible value of  $\phi_L$ , provided  $\phi_L + \phi_R = 0$ . The spontaneous breaking of such a symmetry (in this context facilitated by the presence of random noise) manifests itself through different modulation profiles, as it is evidenced in Fig. 3b. This phase freedom appears to be lost when  $U_{0,1} \neq 0$ , as evidently inferred from Figs. 3c,d.

Finally, in order to quantitatively verify the spontaneous breaking of the phase symmetry for  $U_{0,1} = 0$ , we considered 300 different random evolutions towards the

steady-state. The results of this statistical analysis are reported in Fig. 4. In particular, the absolute value of the Fourier components of  $\Delta^{(j)}(x)$  as a function of  $k_x$  is shown in Fig. 4a for the different randomly generated profiles. In all cases, the Fourier spectrum appears strongly peaked around positive/negative  $k_x$  values, corresponding to the difference between the condensate ( $k_x = 0$ ) and the side peaks on the  $(1, \pm)$  bands located at  $\bar{k}_x \simeq \pm 0.3 \mu\text{m}^{-1}$ , respectively. This is in agreement with the emission spectrum shown in Fig. 2f. However, the phase difference between these (almost) periodic profiles, which evidently appears in Fig. 3d, is a random quantity. This is confirmed by combining the numerical results shown in Figs. 4b and 4c. In Fig. 4b we report the value  $\phi_L^{(j)} + \phi_R^{(j)}$  as a function of  $\phi_L^{(j)}$  for any  $j \in [1, 300]$  ( $\phi_{L/R}^{(j)}$  is the phase corresponding to the Left/Right peak of the Fourier transforms shown in Fig. 4a). By construction,  $\phi_L^{(j)} + \phi_R^{(j)} = 0$ , for any  $j$ . In addition, numerical results show that  $\phi_L^{(j)}$  takes values spanning the whole  $[-\pi, \pi]$  interval. In particular,  $\phi_L^{(j)}$  is uniformly distributed in this range, as evidenced by results shown in Fig. 4c, in which the maximum of the absolute value of these modulations is plotted after averaging over  $N$  different realizations (on increasing  $N$ ), i.e.,

$$|\Delta_N(x)| = \left| \frac{1}{N} \sum_{j=1}^N \Delta^{(j)}(x) \right|. \quad (8)$$

For  $N = 1$ ,  $\text{Max}(|\Delta_N(x)|)$  gives a value compatible with the results already shown in Fig. 4c. However,  $\text{Max}(|\Delta_N(x)|)$  significantly decays on increasing  $N$ , a signature that the different modulation profiles interfere destructively, i.e., that  $\phi_L^{(j)}$  is uniformly and randomly distributed in  $[-\pi, \pi]$ . In other words, outside the region where emission is dominated by the  $m = 0$  mode, the main contribution to the spatial modulation  $\Delta^{(j)}(x)$  behaves as  $\cos(\bar{k}_x \cdot x + \phi_L^{(j)})$ , with  $\bar{k}_x \simeq 0.3 \mu\text{m}^{-1}$ . These results unequivocally show the spontaneous breaking of a phase symmetry in real space, which gives us the ultimate definition of the *polariton supersolid* state.

**Summary.** We have proposed a realistic configuration in which a supersolid state can be observed in the stationary regime of a condensate of exciton-polaritons. We have explicitly pointed out experimentally accessible signatures of the simultaneous breaking of the condensate phase and its spatial symmetries. In addition to the onset of a spatial modulation, we have also identified the presence of a double threshold in the emission from the polariton side-branches as the signatures of a supersolid state on top of the polariton condensate. Besides providing a further platform where such exotic states of matter can be studied, polariton condensates intrinsically differentiate from their atomic counterparts owing to their driven-dissipative nature. As for the standard

non-equilibrium condensation [34], this is anticipated to give peculiar dispersion laws for the Goldstone modes associated to the spontaneously broken symmetries [35–39], with potential consequences onto the long-distance coherence of the corresponding order parameters [40].

**Acknowledgments.** This project was partly funded by the European Union–Next Generation EU within the Italian Ministry of Research (MUR) PNRR project PE0000023-NQSTI. IC acknowledges financial support from the Provincia Autonoma di Trento, from the Q@TN initiative. The authors acknowledge useful scientific discussions with G.I. Martone.

---

\* Corresponding author: [davide.nigro@unipr.it](mailto:davide.nigro@unipr.it)

- [1] D. Sanvitto and S. Kéna-Cohen, The road towards polaritonic devices, *Nature Materials* **15**, 1061 (2016).
- [2] C. Sturm, D. Tanese, H. Nguyen, H. Flayac, E. Galopin, A. Lemaître, I. Sagnes, D. Solnyshkov, A. Amo, G. Malpuech, and J. Bloch, All-optical phase modulation in a cavity-polariton Mach–Zehnder interferometer, *Nature Communications* **5**, 3278 (2014).
- [3] D. G. Suárez-Forero, F. Riminucci, V. Ardizzone, N. Karpowicz, E. Maggiolini, G. Macorini, G. Lerario, F. Todisco, M. D. Giorgi, L. Dominici, D. Ballarini, G. Gigli, A. S. Lanotte, K. West, K. Baldwin, L. Pfeiffer, and D. Sanvitto, Enhancement of Parametric Effects in Polariton Waveguides Induced by Dipolar Interactions, *Physical Review Letters* **126**, 137401 (2021).
- [4] B. Datta, M. Khatoniar, P. Deshmukh, F. Thouin, R. Bushati, S. De Liberato, S. K. Cohen, and V. M. Menon, Highly nonlinear dipolar exciton-polaritons in bilayer MoS<sub>2</sub>, *Nature Communications* **13**, 10.1038/s41467-022-33940-3 (2022).
- [5] J. Kasprzak, M. Richard, S. Kundermann, A. Baas, P. Jeambrun, J. M. J. Keeling, F. M. Marchetti, M. H. Szymańska, R. André, J. L. Staehli, V. Savona, P. B. Littlewood, B. Deveaud, and L. S. Dang, Bose–Einstein condensation of exciton polaritons, *Nature* **443**, 409 (2006).
- [6] A. Amo, J. Lefrère, S. Pigeon, C. Adrados, C. Ciuti, I. Carusotto, R. Houdré, E. Giacobino, and A. Bramati, Superfluidity of polaritons in semiconductor microcavities, *Nature Physics* 10.1038/nphys1364 (2009).
- [7] A. Amo, S. Pigeon, D. Sanvitto, V. G. Sala, R. Hivet, I. Carusotto, F. Pisanello, G. Leménager, R. Houdré, E. Giacobino, C. Ciuti, and A. Bramati, Polariton superfluids reveal quantum hydrodynamic solitons, *Science* **332**, 1167 (2011).
- [8] I. Carusotto and C. Ciuti, Quantum fluids of light, *Rev. Mod. Phys.* **85**, 299 (2013).
- [9] Q. Fontaine, D. Squizzato, F. Baboux, I. Amelio, A. Lemaître, M. Morassi, I. Sagnes, L. Le Gratiet, A. Harouri, M. Wouters, I. Carusotto, A. Amo, M. Richard, A. Minguzzi, L. Canet, S. Ravets, and J. Bloch, Kardar-parisi - zhang universality in a one-dimensional polariton condensate, *Nature* **608**, 687 (2022).
- [10] J. Bloch, I. Carusotto, and M. Wouters, Non-equilibrium bose–einstein condensation in photonic systems, *Nature Reviews Physics* **4**, 470 (2022).
- [11] Y. Yoon, J. Deschamps, M. Steger, K. W. West, L. N. Pfeiffer, D. W. Snoke, and K. A. Nelson, Enhanced thermalization of exciton-polaritons in optically generated potentials, arXiv:2209.13703 (2022).
- [12] Y. Sun, P. Wen, Y. Yoon, G. Liu, M. Steger, L. N. Pfeiffer, K. West, D. W. Snoke, and K. A. Nelson, Bose-Einstein Condensation of Long-Lifetime Polaritons in Thermal Equilibrium, *Physical Review Letters* **118**, 1 (2017).
- [13] C. Schneider, K. Winkler, M. D. Fraser, M. Kamp, Y. Yamamoto, E. A. Ostrovskaya, and S. Höfling, Exciton-polariton trapping and potential landscape engineering, *Reports on Progress in Physics* **80**, 10.1088/0034-4885/80/1/016503 (2017).
- [14] L. Ferrier, E. Wertz, R. Johne, D. D. Solnyshkov, P. Senellart, I. Sagnes, A. Lemaître, G. Malpuech, and J. Bloch, Interactions in confined polariton condensates, *Physical Review Letters* **106**, 10.1103/PhysRevLett.106.126401 (2011).
- [15] E. Wertz, L. Ferrier, D. D. Solnyshkov, R. Johne, D. Sanvitto, A. Lemaître, I. Sagnes, R. Grousson, A. V. Kavokin, P. Senellart, G. Malpuech, and J. Bloch, Spontaneous formation and optical manipulation of extended polariton condensates, *Nature Physics* **6**, 860 (2010).
- [16] D. Gerace and L. C. Andreani, Quantum theory of exciton-photon coupling in photonic crystal slabs with embedded quantum wells, *Phys. Rev. B* **75**, 235325 (2007).
- [17] N. H. M. Dang, D. Gerace, E. Drouard, G. Trippé-Allard, F. Lédée, R. Mazurczyk, E. Deleporte, C. Seassal, and H. S. Nguyen, Tailoring dispersion of room-temperature exciton-polaritons with perovskite-based subwavelength metasurfaces, *Nano Letters*, *Nano Letters* **20**, 2113 (2020).
- [18] S. Zanotti, H. S. Nguyen, M. Minkov, L. C. Andreani, and D. Gerace, Theory of photonic crystal polaritons in periodically patterned multilayer waveguides, *Phys. Rev. B* **106**, 115424 (2022).
- [19] V. Ardizzone, F. Riminucci, S. Zanotti, A. Gianfrate, M. Efthymiou-Tsironi, D. G. Suárez-Forero, F. Todisco, M. De Giorgi, D. Trypogeorgos, G. Gigli, K. Baldwin, L. Pfeiffer, D. Ballarini, H. S. Nguyen, D. Gerace, and D. Sanvitto, Polariton Bose–Einstein condensate from a bound state in the continuum, *Nature* **605**, 447 (2022).
- [20] F. Baboux, D. D. Bernardis, V. Goblot, V. N. Gladilin, C. Gomez, E. Galopin, L. L. Gratiet, A. Lemaître, I. Sagnes, I. Carusotto, M. Wouters, A. Amo, and J. Bloch, Unstable and stable regimes of polariton condensation, *Optica* **5**, 1163 (2018).
- [21] D. Tanese, H. Flayac, D. Solnyshkov, A. Amo, A. Lemaître, E. Galopin, R. Braive, P. Senellart, I. Sagnes, G. Malpuech, and J. Bloch, Polariton condensation in solitonic gap states in a one-dimensional periodic potential, *Nature Communications* **4**, 10.1038/ncomms2760 (2013).
- [22] F. Riminucci, A. Gianfrate, D. Nigro, V. Ardizzone, S. Dhuey, L. Francaviglia, K. Baldwin, L. N. Pfeiffer, D. Ballarini, D. Trypogeorgos, A. Schwartzberg, D. Gerace, and D. Sanvitto, Polariton condensation in gap-confined states of photonic crystal waveguides, *Phys. Rev. Lett.* **131**, 246901 (2023).
- [23] D. Nigro and D. Gerace, Theory of exciton-polariton condensation in gap-confined eigenmodes, *Phys. Rev. B* **108**, 085305 (2023).

- [24] H. Sigurdsson, H. C. Nguyen, and H. S. Nguyen, Dirac exciton–polariton condensates in photonic crystal gratings, *Nanophotonics* doi:10.1515/nanoph-2023-0834 (2024).
- [25] M. Boninsegni and N. V. Prokof'ev, Colloquium: Supersolids: What and where are they?, *Rev. Mod. Phys.* **84**, 759 (2012).
- [26] J. Léonard, A. Morales, P. Zupancic, T. Esslinger, and T. Donner, Supersolid formation in a quantum gas breaking a continuous translational symmetry, *Nature* **543**, 87 (2017).
- [27] L. Tanzi, E. Lucioni, F. Famà, J. Catani, A. Fioretti, C. Gabbanini, R. N. Bisset, L. Santos, and G. Modugno, Observation of a dipolar quantum gas with metastable supersolid properties, *Phys. Rev. Lett.* **122**, 130405 (2019).
- [28] F. Böttcher, J.-N. Schmidt, M. Wenzel, J. Hertkorn, M. Guo, T. Langen, and T. Pfau, Transient supersolid properties in an array of dipolar quantum droplets, *Phys. Rev. X* **9**, 011051 (2019).
- [29] L. Chomaz, D. Petter, P. Ilzhöfer, G. Natale, A. Trautmann, C. Politi, G. Durastante, R. M. W. van Bijnen, A. Patscheider, M. Sohmen, M. J. Mark, and F. Ferlaino, Long-lived and transient supersolid behaviors in dipolar quantum gases, *Phys. Rev. X* **9**, 021012 (2019).
- [30] A. Recati and S. Stringari, Supersolidity in ultracold dipolar gases, *Nature Reviews Physics* **5**, 735 (2023).
- [31] D. Gerace and L. C. Andreani, Gap maps and intrinsic diffraction losses in one-dimensional photonic crystal slabs, *Phys. Rev. E* **69**, 056603 (2004).
- [32] D. Bajoni, D. Gerace, M. Galli, J. Bloch, R. Braive, I. Sagnes, A. Miard, A. Lemaître, M. Patrini, and L. C. Andreani, Exciton polaritons in two-dimensional photonic crystals, *Phys. Rev. B* **80**, 201308 (2009).
- [33] M. Wouters, I. Carusotto, and C. Ciuti, Spatial and spectral shape of inhomogeneous nonequilibrium exciton-polariton condensates, *Phys. Rev. B* **77**, 115340 (2008).
- [34] F. Claude, M. J. Jacquet, M. Wouters, E. Giacobino, Q. Glorieux, I. Carusotto, and A. Bramati, Observation of the diffusive nambu-goldstone mode of a nonequilibrium phase transition (2023), arXiv:2310.11903 [cond-mat.quant-gas].
- [35] L. Tanzi, S. M. Roccuzzo, E. Lucioni, F. Famà, A. Fioretti, C. Gabbanini, G. Modugno, A. Recati, and S. Stringari, Supersolid symmetry breaking from compressional oscillations in a dipolar quantum gas, *Nature* **574**, 382 (2019).
- [36] M. Guo, F. Böttcher, J. Hertkorn, J.-N. Schmidt, M. Wenzel, H. P. Büchler, T. Langen, and T. Pfau, The low-energy goldstone mode in a trapped dipolar supersolid, *Nature* **574**, 386 (2019).
- [37] G. Natale, R. M. W. van Bijnen, A. Patscheider, D. Petter, M. J. Mark, L. Chomaz, and F. Ferlaino, Excitation spectrum of a trapped dipolar supersolid and its experimental evidence, *Phys. Rev. Lett.* **123**, 050402 (2019).
- [38] J. Léonard, A. Morales, P. Zupancic, T. Donner, and T. Esslinger, Monitoring and manipulating higgs and goldstone modes in a supersolid quantum gas, *Science* **358**, 1415 (2017).
- [39] K. T. Geier, G. I. Martone, P. Hauke, and S. Stringari, Exciting the goldstone modes of a supersolid spin-orbit-coupled bose gas, *Phys. Rev. Lett.* **127**, 115301 (2021).
- [40] R. Daviet, C. P. Zelle, A. Rosch, and S. Diehl, Nonequilibrium criticality at the onset of time-crystalline order, *Phys. Rev. Lett.* **132**, 167102 (2024).